scientific reports

Check for updates

OPEN

Identifying novel aging-related diagnostic and prognostic models and aging-targeted drugs for sepsis patients

Kai Yang[1,2,3,6], Yaoyao Lu[4,6], Jian Gu[1,2,3], Yingli Nie[5]✉ & Tao Zhang[1,2,3]✉

Sepsis is defined as a dysfunctional, life-threatening response to infection leading to multiorgan dysfunction and failure. During the past decade, studies have highlighted the relationship between sepsis and aging. However, the role of aging-related mechanisms in the progression and prognosis of sepsis remains unclear. In the present study, we divided sepsis patients into High- and Low-aging groups based on the gene set variation analysis (GSVA) scores of GOBP-AGING gene set. Sepsis patients in the high-aging group exhibited higher levels of infiltration of innate immune cells, lower levels of infiltration of adaptive immune cells, and a worse prognosis than those in the Low-aging group. Additionally, the MPO to MME ratio (MPO/MME) appears to be an effective biomarker for predicting the prognosis of sepsis patients. Moreover, ARG1/SEC63 and ARG1/CDKN1C appear to be effective and robust biomarkers for the early diagnosis of sepsis patients. Finally, we found that thalidomide (TAL) significantly ameliorated LPS induced inflammation and organ injury and attenuated LPS induced cellular senescence in lung and kidney. Overall, this study provides new insights into the heterogeneity of sepsis, reveals the vital role of aging-related markers in the prognosis and diagnosis of sepsis and demonstrates that TAL is a novel aging-targeted drug for sepsis patients by attenuating LPS induced cellular senescence.

Keywords Sepsis, Aging, Classification, Prognosis, Diagnosis, Thalidomide

Sepsis is a heterogeneous and imprecise syndrome that includes a wide variety of heterogeneous nonspecific clinical manifestations. Over the last decade, there have been advances in the use of high-throughput techniques to improve the definition, early diagnosis, subtype classification, prognostication, and personalization management of sepsis[1]. Baghela et al. stratified early sepsis into five distinct endotypes, including neutrophilic suppressive/NPS, inflammatory/INF, innate-host-defense/IHD, interferon/IFN, and adaptive/ADA, each endotype with unique gene expression profiles, distinct mechanisms, and different manifestations[2]. Scicluna et al. identified four molecular endotypes for sepsis, namely, Mars1-4. Among the four endotypes, sepsis patients in the Mars1 subtype have the worst prognosis[3]. Davenport et al. defined two distinct sepsis response signatures (SRS1 and SRS2) based on the transcriptomic analysis of peripheral blood leucocytes. Patients with SRS1 exhibited an immunosuppressed phenotype with a worse prognosis than patients with SRS2[4]. The detection of sepsis endotypes significantly improved the personalized management of sepsis patients.

During the past decade, several studies have demonstrated that sepsis functions as a stress factor inducing senescence or aging in several tissues[5]. In both in vivo and in vitro lipopolysaccharide (LPS), human respiratory syncytial virus (hRSV), and avian H7N9 influenza virus-induced sepsis models, senescence markers were significantly elevated, including senescence-associated-β-galactosidase (SA-β-Gal) activity, the expression of p16, p21, and p53, senescence-associated secretory phenotype (SASP), and telomere shortening[6–10]. Moreover,

[1]Department of Anesthesiology, Union Hospital, Tongji Medical College, Huazhong University of Science and Technology, Wuhan 430022, China. [2]Key Laboratory of Anesthesiology and Resuscitation, Ministry of Education, Huazhong University of Science and Technology, Wuhan, China. [3]Institute of Anesthesia and Critical Care Medicine, Union Hospital, Tongji Medical College, Huazhong University of Science and Technology, Wuhan 430022, China. [4]Department of Gastrointestinal Surgery, Union Hospital, Tongji Medical College, Huazhong University of Science and Technology, Wuhan 430022, China. [5]Department of Dermatology, Wuhan Children's Hospital (Wuhan Maternal and Child Healthcare Hospital), Tongji Medical College, Huazhong University of Science and Technology, Wuhan 430014, China. [6]Kai Yang and Yaoyao Lu contributed equally to thid work. ✉email: yingli_nie@163.com; 2019xh0150@hust.edu.cn

Oliveira et al. first found in humans that telomere length was significantly shortened 1 week after the initiation of sepsis[11]. Furthermore, Merdji et al. recently found that the senescence of endothelial and vascular cells induced by sepsis was associated with long-term cardiovascular complications, such as acute heart failure, myocardial infarction, or stroke[12]. However, no study has explored the molecular classification of sepsis related to senescence or aging. The prognostic value of senescence- or aging-related genes in sepsis also remains unclear.

Senescence and aging play important roles in the pathogenesis and long-term outcome of sepsis. In the present study, we constructed a novel molecular classification based on aging-related genes, and two subgroups of sepsis, namely, High-aging and Low-aging, were identified. We then evaluated the clinical features, transcriptome features, and immune infiltration of the two sepsis subclasses. Additionally, the least absolute shrinkage and selection operation (LASSO)-Cox regression and LASSO-binomial regression were used to screen key genes for constructing prognostic and diagnostic models for sepsis patients[13]. Finally, we screened and validated aging-targeted drugs based on aging-related differentially expressed genes (DEGs) for sepsis patients using the connective map (cMap) database and LPS induced mice model of sepsis.

Results

Two sepsis groups were identified according to the GSVA scores of the GOBP_AGING gene set

To explore the role of senescence or aging in the progression and outcome of sepsis patients, we estimated the activity of senescence- or aging-related gene sets in sepsis patients by GSVA. As shown in Fig. 1A,B, the GOBP_AGING scores were markedly elevated in sepsis patients compared to normal controls. Moreover, we performed scRNA-seq analysis to depict the landscape of senescence in different cell types of PBMC samples from human sepsis (Fig. 1C). Compared to healthy controls, the scores of GOBP_AGING were significantly elevated in sepsis blood samples in the major cell types of human PBMCs, including $CD4^+$ T cells (Fig. 1D), monocytes (Fig. 1E), and B cells (Fig. 1F). According to the median value of the GSVA score, the sepsis patients in GSE68652 were divided into High- and Low-aging groups (Fig. 1G), and the outcome of patients in different groups is shown in Fig. 1H. Moreover, other aging-related gene sets were also found to be significantly increased in the High-aging group, including oxidative stress-induced senescence, kynurenine pathway and links to cell senescence, COVID-19 and endothelial cell senescence, aging, multicellular organism aging, and replicative senescence. In contrast, the negative regulation of cellular senescence was markedly decreased in the High-aging group (Fig. 1I).

Subsequently, we further investigated the clinical features of the two sepsis subclasses. As shown in Fig. 2A, patients in the High-aging group had a worse prognosis than those in the Low-aging group. Moreover, there was also a tendency for more patients to die in the High-aging group from the GSE26440-26378 and E-NTAB-4421 cohorts. However, that tendency happened to be statistically insignificant using the available data set (Fig. 2B,C and Supplementary table 2). In addition, we compared our categorization to previously identified sepsis endotypes, including Baghela's signature (neutrophilic suppressive/NPS, inflammatory/INF, innate-host-defense/IHD, interferon/IFN, and adaptive/ADA) and Scicluna's signature (Mars1-4). As shown in Fig. 2D and Supplementary table 3, the High-aging group was significantly associated with Baghela's inflammatory and Scicluna's Mars1 subtypes. Conversely, the Low-aging group was significantly associated with Baghela's Neutrophilic Supressive, InnateHost Def, and Adaptive, and Scicluna's Mars2 and Mars4 subtypes (Fig. 2E and Supplementary table 3).

Transcriptome features of the aging-related sepsis groups

Differential analyses were conducted to comprehend the distinctions in the molecular and biological processes among the two sepsis subclasses using the "limma" R package. Significant differences in gene expression were defined as $|\log2FC| > 0.2$ and adjusted P value < 0.05. A total of 202 DEGs, including 187 up-regulated and 15 down-regulated DEGs for the High-aging group, were identified (Supplementary table 4).

Next, functional enrichment analysis of the up-regulated DEGs was performed utilizing the Metascape database, and 68 remarkably enriched biological processes or pathways (adjusted P value < 0.05) are shown in Supplementary table 5. The up-regulated DEGs of the High-aging cluster were enriched in processes or pathways related to erythrocyte differentiation, proteolysis involved in protein catabolic processes, erythrocytes taking up oxygen and releasing carbon dioxide, regulation of autophagy, heme biosynthesis, inorganic ion homeostasis, negative regulation of extrinsic apoptotic signaling pathways, hematopoietic stem cell differentiation, regulation of protein catabolic processes, metabolic reprogramming in pancreatic cancer, arginine and proline metabolism, multicellular organismal-level iron ion homeostasis, hemoglobin metabolic processes, oxygen transport, and negative regulation of protein polymerization (Supplementary table 5).

Moreover, to further investigate the molecular characteristics of the aging-related sepsis subclasses, hallmark gene sets were chosen and quantified using the GSVA algorithm, which consists of eight distinct process categories and provides precise but comprehensive inputs for gene set enrichment analysis[14]. The results are presented in a heatmap (Fig. 3A). The High-aging group exhibited the highest levels of pathways, including hypoxia, myogenesis, epithelial mesenchymal transition, xenobiotic metabolism, reactive oxygen species pathway, p53 pathway, UV response up, angiogenesis, haem metabolism, coagulation, and KRAS signaling up, compared to the low-aging group and normal controls (Fig. 3B). On the contrary, the High-aging group exhibited the lowest levels of pathways, including DNA repair, unfolded protein response, E2F targets, MYC targets v1, allograft rejection, and pancreas β cells, compared to the Low-aging group and normal controls (Fig. 3C).

Immune cell infiltration and immune function levels of the aging-related sepsis groups

Given the significant roles of immune processes in the pathogenesis of sepsis, immune cell infiltration and immune function were estimated to characterize the immunological landscape of the aging-related sepsis

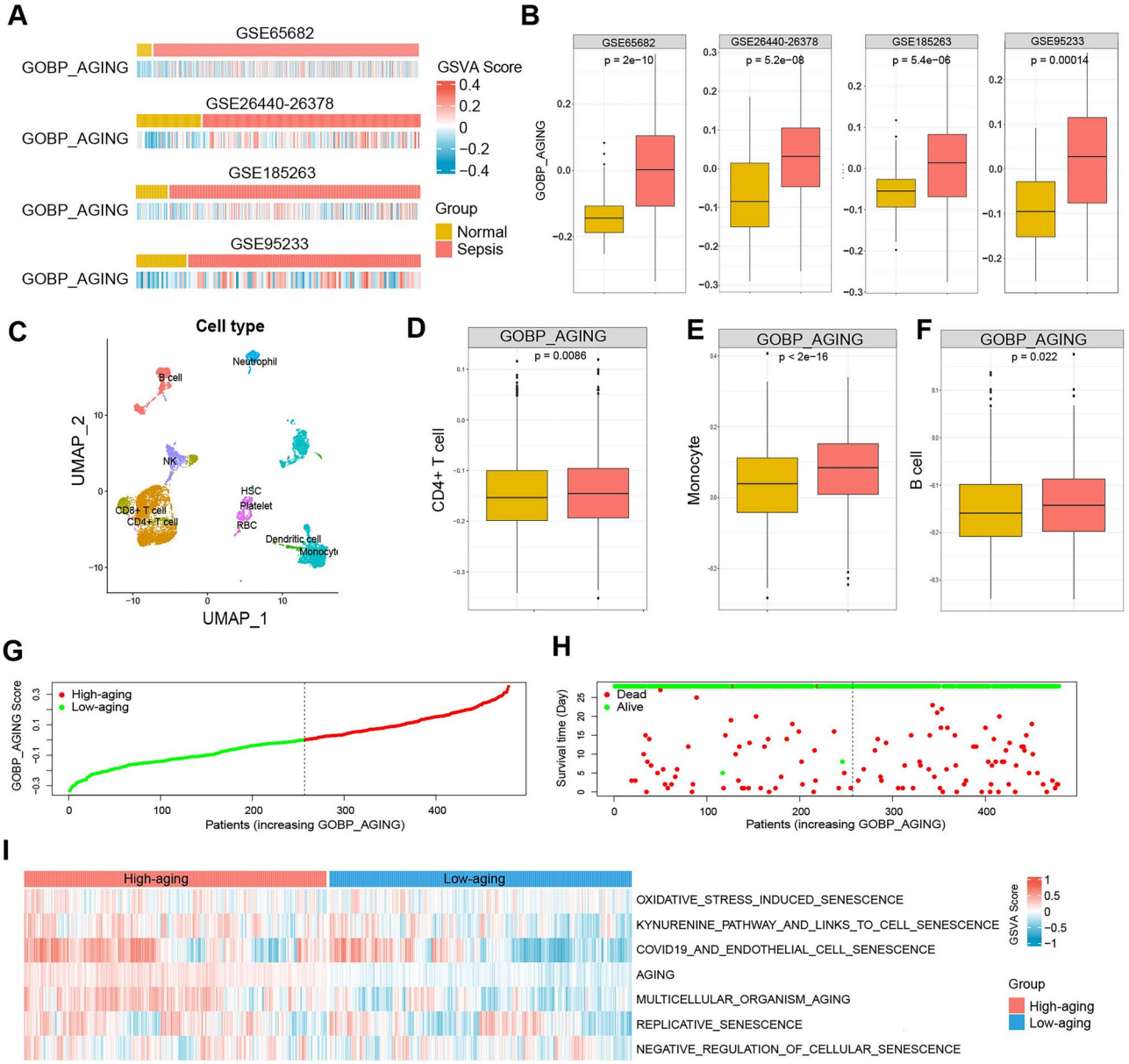

Fig. 1. Two sepsis groups were identified according to the GSVA scores of the GOBP_AGING gene set. (**A**,**B**) GSVA scores of the GOBP_AGING gene set were significantly higher in sepsis patients than in normal controls from GSE65682, GSE26440-26378, GSE185263, and GSE95233. (**C**) UMAP visualization of different cell types from human PBMCs. Comparison of GOBP_AGING scores between sepsis patents and healthy controls in CD4 + T cells (**D**), monocytes (**E**), and B cells (**F**). (**G**) Sepsis patients from GSE68682 were divided into High- and Low-aging groups according to the median score of the GOBP_AGING. (**H**) The outcome of sepsis patients in the two sepsis groups. (**I**) GSVA scores of aging-related gene sets were significantly higher in the High-aging group than in the Low-aging group from GSE65682. *GSVA* gene set variation analysis.

groups. As shown in Fig. 4A, the scores of adaptive immune response-associated signatures were significantly reduced in the High-aging group compared to the Low-aging and normal control groups, including various gene sets in the categories of T cells and B cells. In contrast, innate immune response-associated signatures were significantly elevated in the High-aging group compared to the low-age and normal control groups, including various gene sets in the categories of cytokines, chemokines, dendritic cells, macrophages, and neutrophils (Fig. 4B). Moreover, the adaptive immune response-associated signatures were highly negatively correlated with the GSVA scores of GOBP_AGING. The innate immune response-associated signatures were highly positively correlated with the GSVA scores of GOBP_AGING (Fig. 4C).

Construction of aging-related sepsis-DEG-based prognostic model

To further construct an aging-related prognostic model for sepsis patients, we first screened 1700 up-regulated and 1624 down-regulated sepsis-related common DEGs by intersecting the up-regulated and down-regulated

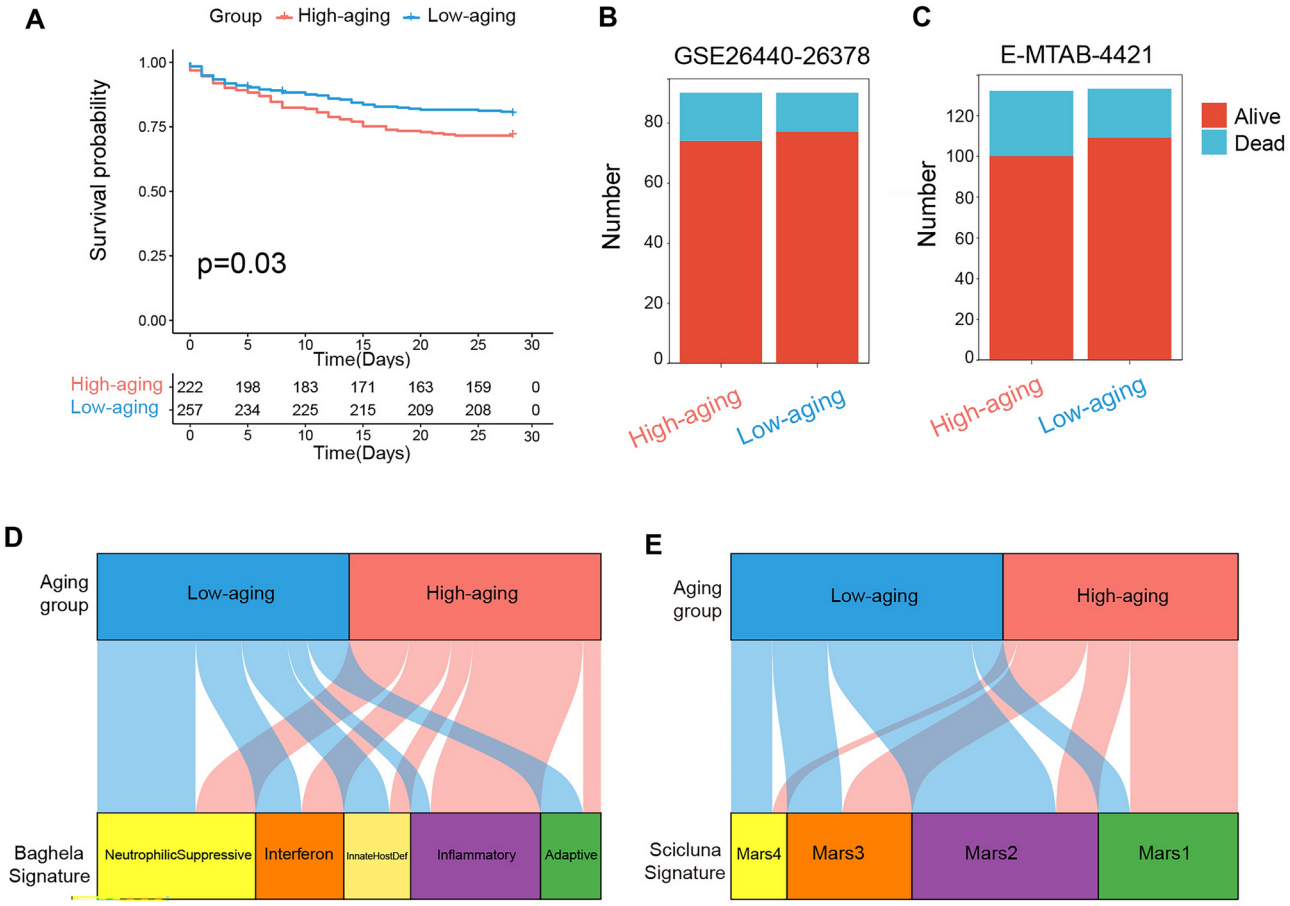

Fig. 2. Clinical features of the aging-related sepsis groups. (**A**) Kaplan–Meier survival analysis of the overall survival of the two sepsis groups from GSE65682. (**B**,**C**) The outcome of sepsis patients in two groups from GSE16440-26378 and E-MTAB-4421. (**D**,**E**) Correlation of the two groups with sepsis endotypes published previously by Baghela[2] and Scicluna[3].

DEGs of sepsis patients compared to heathy controls from GSE68652, GSE185263, GSE95233, and GSE26440-26378, respectively (Fig. 5A and Supplementary table 6). Then, a total of 1517 prognostic genes of sepsis were identified by univariate Cox regression based on GSE65682 cohort (Supplementary table 7). A total of ten aging-related prognostic DEGs were identified by intersecting common DEGs, prognostic genes, and members of the GOBP_AGING gene set, including nine up-regulated genes (ARG1, AURKB, C1QA, EDNRB, GJB6, INHBA, MPO, RETN, and TYMS) and a down-regulated gene (MME) (Fig. 5A).

Then, tenfold LASSO cross-validation Cox regression analysis was conducted to choose the most useful up-regulated prognostic biomarkers for constructing a prognostic classifier based on the nine up-regulated aging-related prognostic DEGs (Fig. 5B). A total of five genes (MPO, AURKB, ARG1, EDNRB, and MME) were identified to construct the prognostic model. All four up-regulated genes were significantly up-regulated in patients with sepsis compared with normal controls (Fig. 5C) and were found to be related to the unfavorable prognosis of sepsis with hazard ratios (HRs) > 1 (Fig. 5C). In contrast, the down-regulated gene, MME, was significantly down-regulated in patients with sepsis compared with normal controls (Fig. 5C) and was found to be related to the favorable prognosis of sepsis with HR < 1 (Fig. 5C).

We constructed a prognostic model using the ratio of up-regulated genes to down-regulated genes. As shown in Fig. 5D, the prognostic value of MPO/MME was higher than that of the other models and may be a promising biomarker for predicting the prognosis of sepsis. As shown in Fig. 5E, time-dependent ROC analysis showed that the area under the curve (AUC) was 0.67, 0.62, and 0.61 for 7, 14, and 28 day survival, respectively. Moreover, patients were further divided into high and low groups according to the optimal cutoff value of MPO/MME (1.050) for predicting 28-day survival. As shown in Fig. 5F, patients in the high group had a worse prognosis than those in the low group. Furthermore, the prognostic significance of the MPO/MME (1.050) model was further validated by external cohorts from different array platforms, including E-MTAB-5273, E-MTAB-5274, and GSE95233. The results showed that the number of sepsis deaths was significantly higher in the high group than in the low group (Fig. 5G and Supplementary table 8).

Finally, the subclass prediction was repeated with the MPO/MME in GSE65682 dataset. The results showed that the concordance of 68.2% in High-Aging subclass and 68.2% in Low-Aging subclasses, suggesting that the MPO/MME can reproducibly determine the sepsis classification (Supplementary Fig. 1).

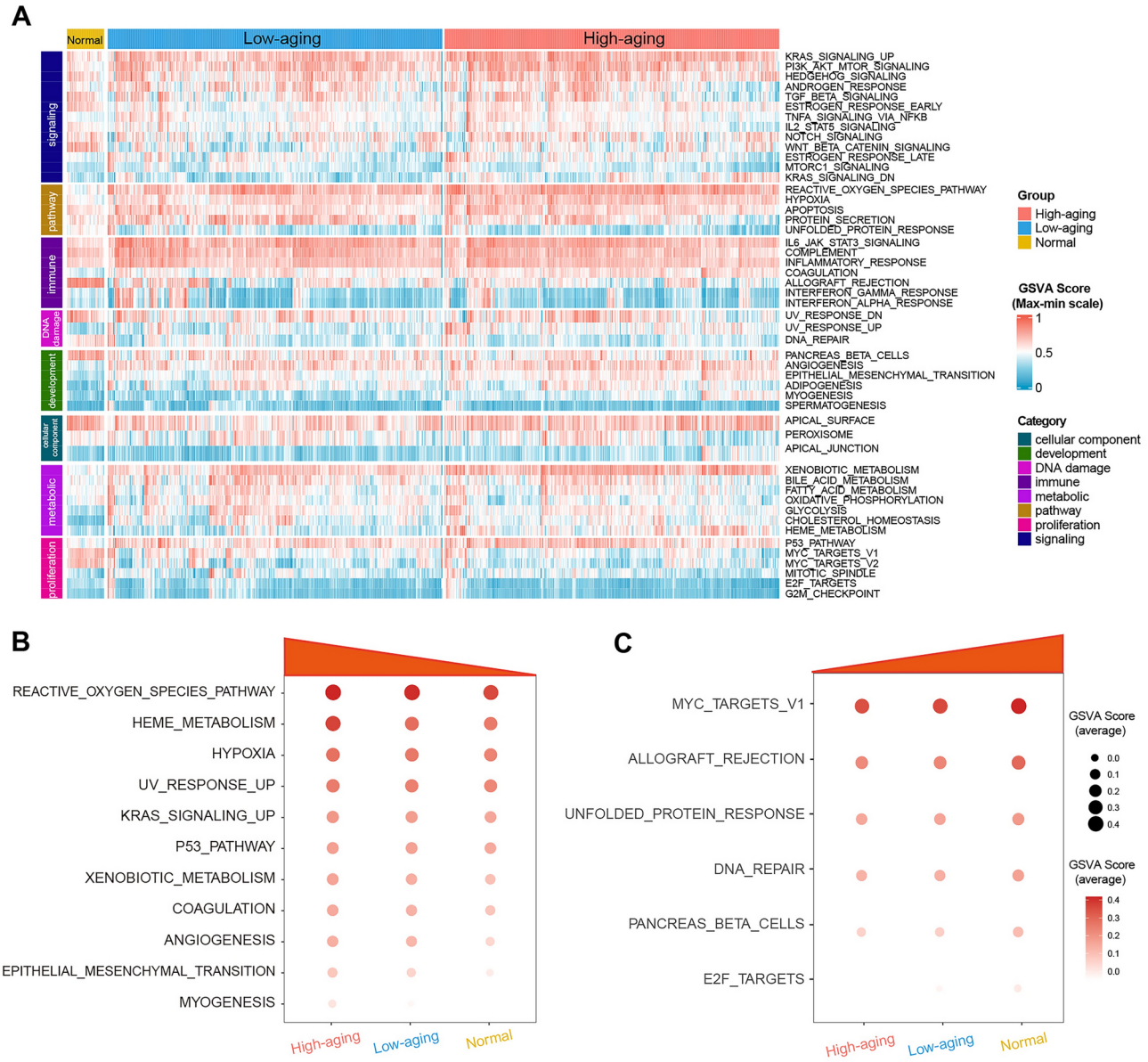

Fig. 3. Transcriptome features of the aging-related sepsis groups. (**A**) The heatmap plot shows the GSVA score of 50 hallmark gene sets of the two sepsis groups and normal controls. The up-regulated (**B**) and down-regulated (**C**) processes or pathways in the High-aging group.

Construction of an aging-related sepsis DEG-based diagnostic model

To further construct an aging-related diagnostic model for sepsis patients, we first screened 25 up-regulated and 14 down-regulated aging-related DEGs by intersecting the up-regulated or down-regulated common DEGs with members of the GOBP_AGING gene set, respectively. Then, LASSO-binomial regression was used to select the most important genes. Finally, a total of eight key genes were identified, including six up-regulated genes (TSPO, ADM, GCLM, CTNNA1, RETN, and ARG1) and two down-regulated genes (SEC63 and CDKN1C) (Fig. 6A, Supplementary table 9).

Similar to the prognostic model, we constructed a diagnostic model using the ratio of up-regulated genes to down-regulated genes. As shown in Fig. 6B, according to the ROC curves, ARG1/SEC63 and ARG1/CDKN1C had the best diagnostic value in the diagnosis of sepsis, with AUC = 0.996 in the GSE65682 cohort. Moreover, the optimal cutoff values were 1.036 and 1.026 for ARG1/SEC63 and ARG1/CDKN1C according to the maximum Youden index[15], respectively (Fig. 6C). Furthermore, the diagnostic significance of both ARG1/SEC63 (1.026) and ARG1/CDKN1C (1.036) was further validated in GSE95233, GSE26440-26,438, and GSE185263 from different array platforms and detection methods (Fig. 6D).

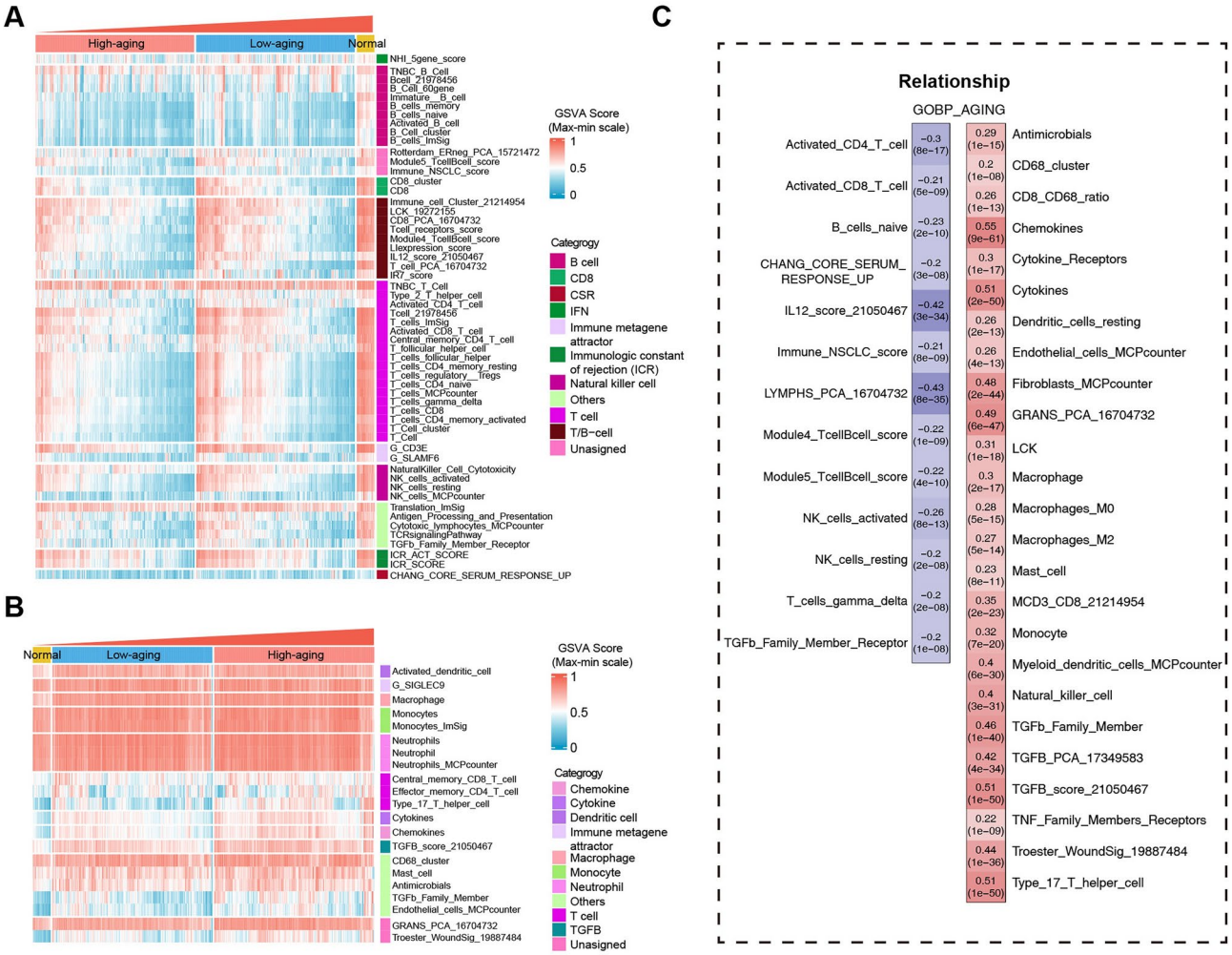

Fig. 4. Immune cell infiltration and immune function levels of the aging-related sepsis groups. The up-regulated (**A**) and down-regulated (**B**) immune cell infiltration or immune function levels in the High-aging group. (**C**) Correlation between immune cell infiltration or immune function levels and GSVA scores of GOBP_AGING.

Thalidomide attenuated lung and kidney injury in LPS induced sepsis mice model

The process of aging-targeted candidate drug identification is shown in (Fig. 7A). A total of 25 up-regulated aging-related DEGs and 14 down-regulated aging-related DEGs were first screened and then uploaded to the cMap database. Thalidomide (TAL) with a low score (−94.36) was identified as an aging-targeted candidate drug for sepsis patients. To further validate the protective role of TAL on sepsis, we performed in vivo experiments using LPS-induced mice model of sepsis. And the procedure of the experiments was shown in (Fig. 7B). As shown in Fig. 7C,D, TAL administration significantly reduced the levels of inflammatory factors. Since lung and kidney are vulnerable to the injury induced by sepsis, we further exam the protective role of TAL on lung and kidney injury. As shown in Fig. 7E, HE staining revealed that administration of TAL ameliorated leukocyte infiltration, pulmonary edema, destruction of alveolar septum, and thus alleviated LPS induced lung injury. Furthermore, TAL administration attenuated renal tubular injury induced by LPS. Moreover, TAL administration significantly attenuated serum levels of creatinine and BUN (Fig. 7F,G), reduced the expression of renal damage markers KIM-1 and NGAL (Fig. 7H).

TAL ameliorated cellular senescence of lung and kidney in LPS induced sepsis mice model

Since TAL was identified as an aging-targeted candidate drug for sepsis patients, we further explore the role of TAL on cellular senescence. As shown in Fig. 8, LPS injection significantly induced cellular senescence in lung and kidney with the elevation of senescence markers p16 and p21. However, TAL administration remarkedly reduced the level of these senescence markers, thus alleviated LPS induced cellular senescence.

Discussion

Sepsis is a common and consequential disease in critically ill patients. Unfortunately, the high heterogeneity of sepsis at the individual level has hindered therapeutic progress. This complexity has prompted attempts to

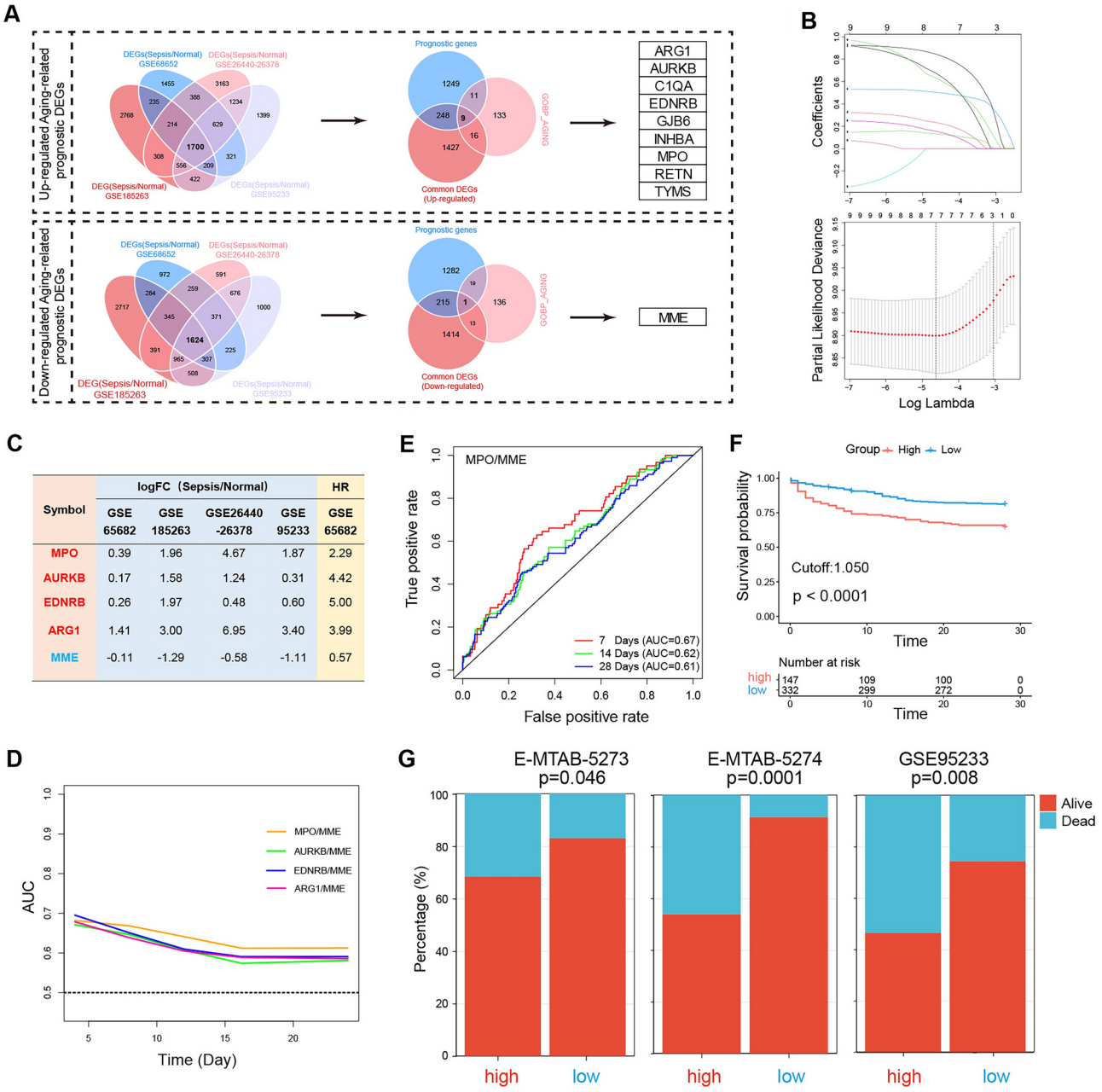

Fig. 5. Construction of an aging-related sepsis DEG-based prognostic model. (**A**) Flow chart of the process of the identification of aging-related prognostic DEGs. (**B**) Results of LASSO Cox regression screening of four genes that are essential for the prognosis of sepsis. The upper panel shows the shrinkage profile of LASSO coefficients. The lower panel is the cross-validation plot of LASSO. (**C**) Gene expression changes and HR of all five genes from GSE65682, GSE185263, GSE95233, and GSE26440-26378. (**D**) The AUCs of different models in predicting the survival of sepsis patients within 28 days. (**E**) The time-dependent ROC for 7, 14, and 28 day overall survival predictions for the MPO/MME. (**F**) Kaplan–Meier survival analysis of overall survival of the high and low groups divided by the value of MPO/MME (1.050) from GSE65682. (**G**) The outcome of sepsis patients in the high and low groups from MTAB-5273, E-MTAB-5274, and GSE95233. *LASSO* least absolute shrinkage and selection operation, *FC* fold change, *HR* hazard ratio, *DEGs* differentially expressed genes, *AUC* area under the curve, *ROC* receiver operating characteristic curve.

develop a precision medicine approach by classifying patients into more homogeneous subtypes with shared biological and clinical features[16].

In the present study, we constructed a novel molecular classification based on aging-related genes, and High-aging and Low-aging subtypes were identified. Patients in the High-aging group had a high level of aging-related pathways with a worse prognosis than those in the Low-aging group. Moreover, the two groups showed distinct transcriptome and immune infiltration features. The High-aging group was more enriched in the processes

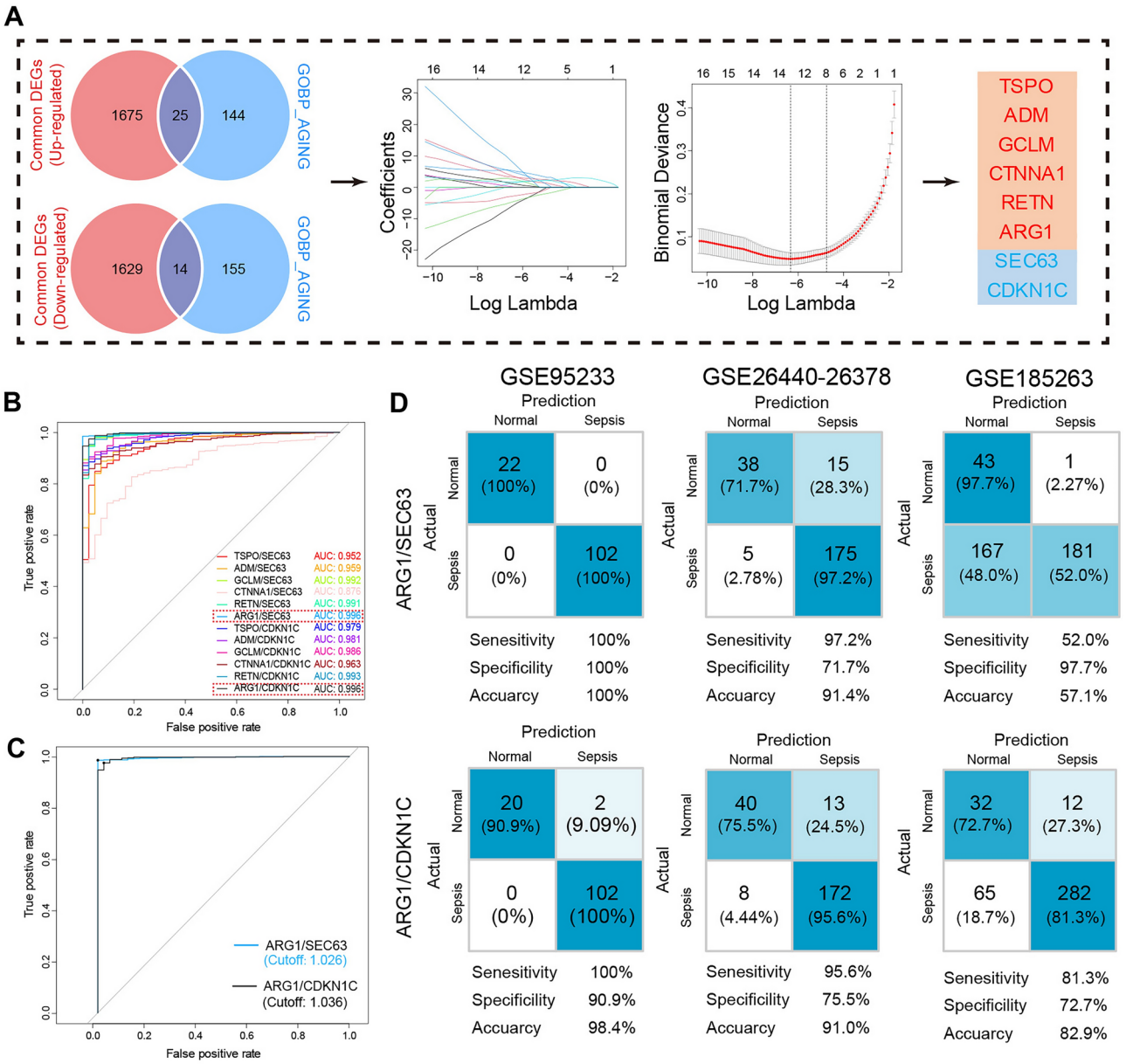

Fig. 6. Construction of an aging-related sepsis-DEG-based diagnostic model. (**A**) Flow chart of the process of the identification of aging-related DEGs. (**B**) The performance of the models in the diagnosis of sepsis patients in the GSE65682 cohort. (**C**) The optimal cutoff values of ARG1/SEC63 and ARG1/CDNK1C. (**D**) The diagnostic value of ARG1/SEC63 (1.036) and ARG1/CDNK1C (1.026) in the external cohorts GSE95233, GSE26440-26378, and GSE185263.

associated with the reactive oxygen species pathway, haem metabolism, and hypoxia than the Low-aging group. In contrast, MYC targets-v1, allograft rejection, and unfolded protein response were notably decreased in the High-aging group. In addition, the High-aging group featured notably increased innate immune response-associated signatures and significantly reduced adaptive immune response-associated signatures compared to the Low-aging and normal control groups.

Furthermore, we compared the correlation between our groups and previously published sepsis endotypes, which provided us with abundant characteristic information related to our novel aging-associated groups, leading to a deeper understanding of our groups. The results demonstrated that the High-aging group was significantly associated with Baghela's inflammatory (INF) and Scicluna's Mars1 subtypes. Conversely, the Low-aging group was significantly associated with Baghela's neutrophilic suppressive (NPS), InnateHostDef (IHD), Adaptive (ADA), and Scicluna's Mars2 and Mars4 subtypes. The NPS endotype was characterized by poor prognosis and nascent immunosuppression with increased neutrophil proportions and downregulation of certain adaptive signaling pathways[2]. The ADA endotype was notable for upregulation of adaptive immune pathways and more abundant lymphocytes. The IHD endotype showed the upregulation of innate host defense, including interleukin

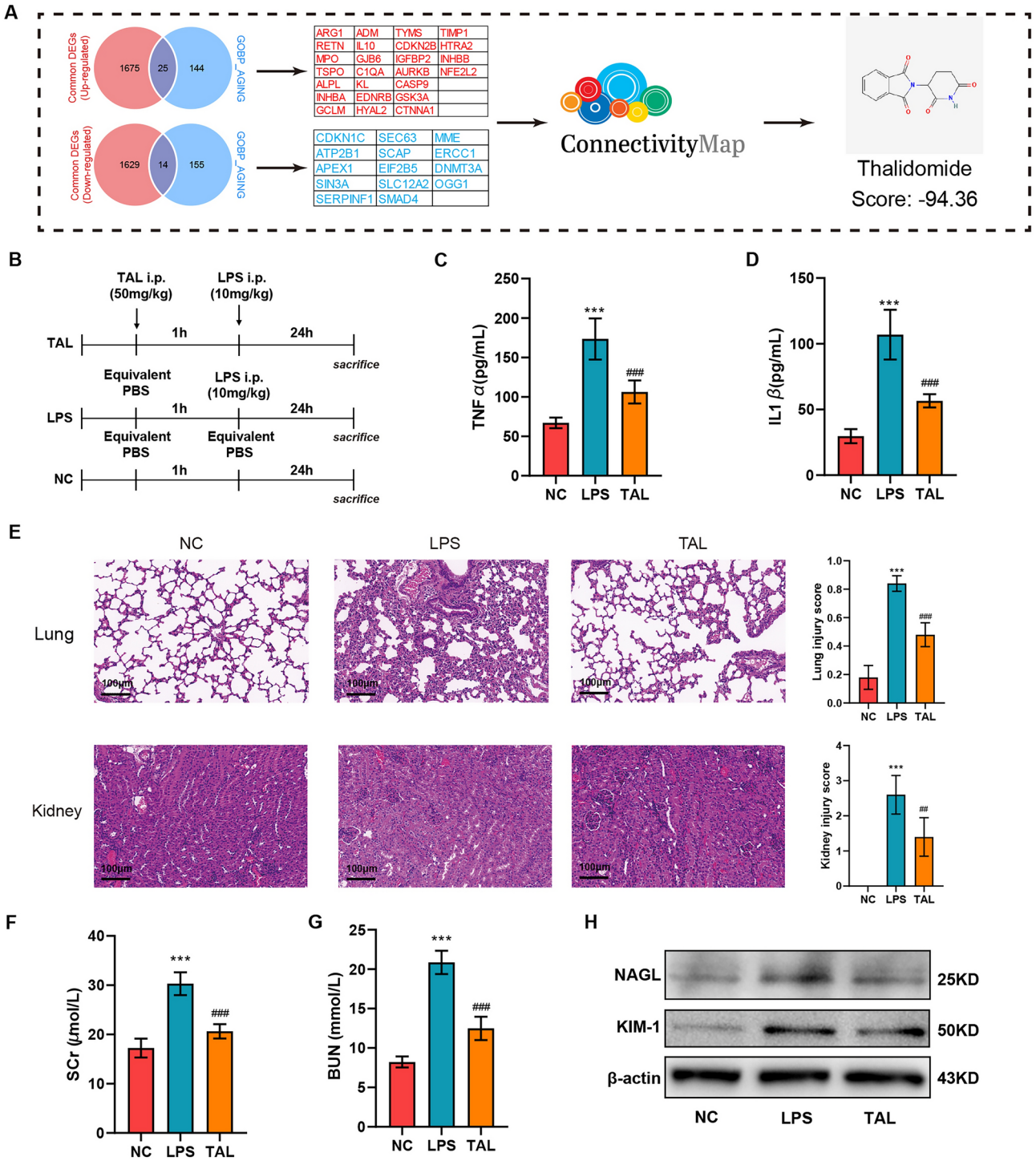

Fig. 7. TAL attenuated lung and kidney injury in LPS induced sepsis mice model (**A**) Flow chart of the process of candidate small-molecule drug identification. (**B**) Experimental design for establishing LPS-induced sepsis mice model and assessing the effect of TAL treatment. Serum levels of TNF-α(**C**) and IL-1β (**D**) from negative control (NC) and LPS induced sepsis mice with TAL or vehicle administration. ***P < 0.001 vs NC group; ###P < 0.001 vs LPS group. (**E**) Representative lung and kidney sections stained with HE from NC and LPS induced sepsis mice with TAL or vehicle administration. Scale: 100 μm. Serum levels of creatinine (**F**) and BUN (**G**) from NC and LPS induced sepsis mice with TAL or vehicle administration. ***P < 0.001 vs NC group; ###P < 0.001 vs LPS group. (**H**) Expression level of KIM-1 and NAGL in kidney tissues from NC and LPS induced sepsis mice with TAL or vehicle administration.

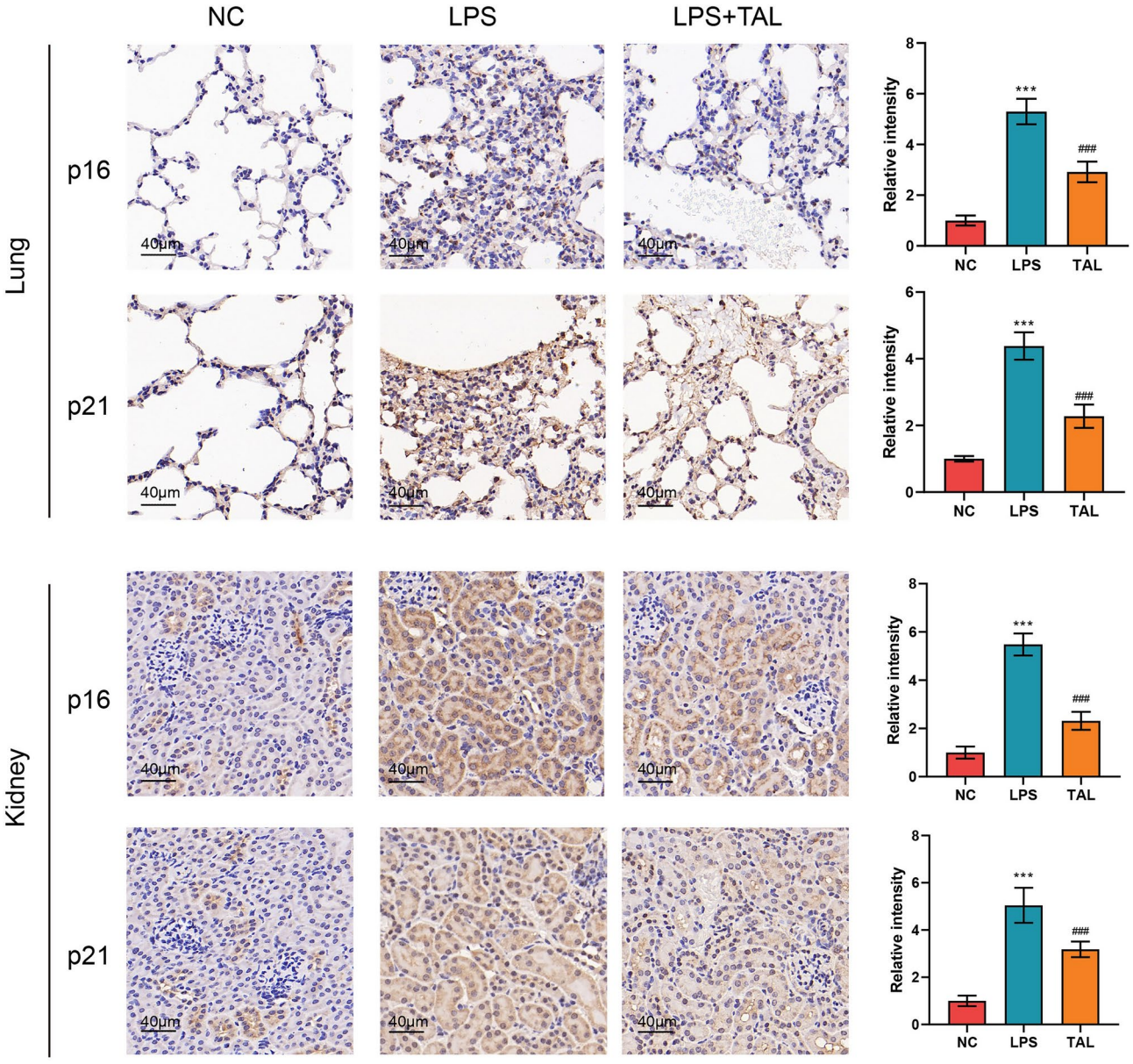

Fig. 8. TAL ameliorated cellular senescence of lung and kidney in LPS induced sepsis mice mode. Representative IHC staining of p16 and p21 f. from NC and LPS induced sepsis mice with TAL or vehicle administration. Scale: 40 μm.

signaling[2]. The INF endotype was similar to the NPS endotype but showed increased inflammatory responses and activation of nuclear factor κB (NF-κB) and TCR/BCR signaling[2]. The Mars1 endotype was associated with the highest mortality, and the poor prognosis was related to a marked decrease in innate and adaptive immune functions such as Toll-like receptor, NF-κB signaling, antigen presentation, and T-cell receptor signaling, concomitant with increased metabolic pathways, including heme biosynthesis pathways[3]. Conversely, the Mars2 endotype was characterized by an increase in pattern recognition, cytokine, cell growth, and mobility pathways[3]. The Mars4 endotype had a lower risk than Mars1, which showed a significant association with increased pattern recognition and cytokine pathways, specifically interferon signaling, TREM1, and RIG1-like receptor signaling[3].

Additionally, we constructed a prognostic model, MPO/MME, with a cutoff value of 1.050, and two diagnostic models, ARG1/SEC63 and ARG1/CDKN1C, with cutoff values of 1.036 and 1.026, respectively. These models performed well and robustly in predicting the prognosis of sepsis patients or diagnosing sepsis. Myeloperoxidase (MPO) is the most abundant granule protein released from neutrophils and monocytes and may be a marker of neutrophil proliferation and the severity of inflammation[17]. MPO-derived toxic oxidant production, such as hypochlorous acid (HOCl), can induce cellular senescence[18]. A previous study demonstrated that MPO increased significantly in sepsis compared with systemic inflammatory response syndrome or healthy controls[19]. Moreover, MPO-derived 2-chlorofatty acids (2-ClFA) contributed to the mortality of sepsis patients by inducing pulmonary endothelial injury and resultant acute respiratory distress syndrome (ARDS)[20]. Membrane metallo-

endopeptidase (MME/Neprilysin/CD10/CALLA) is an extracellular, membrane-bound protease that can target the degradation of a variety of peptides, which play a role in organ development, aging, and diseases of old age[21]. Early in 1995, Lu et al. found that MME might exert a significant protective role in sepsis and that MME-knockout mice exhibited enhanced lethality to endotoxin shock[22]. Moreover, Martens et al. first found that the expression of MME significantly decreased in sepsis patients compared with patients with a systemic viral infection and healthy controls[23]. High MME^{dim} ($CD10^{dim}$) granulocyte proportions predicted clinical deterioration of sepsis patients and were associated with low survival rates[24]. The possible mechanism may be the fact that decreased expression of MME on granulocytes is an important feature of immature myeloid cells, which may have important innate functions in sepsis[25]. Arginase 1 (ARG1) is an arginase that can be released from human granulocytes and maintain high activity in the extracellular space during the inflammatory process[26]. ARG1 is significantly increased in sepsis patients and can act as a promising biomarker for sepsis diagnosis and prognosis[27,28]. The underlying mechanisms may be the fact that ARG1 exerts a profound suppressive effect on immunity through downregulating the expression of T-cell receptor (TCR) and MHC class II molecules[26]. Moreover, ARG1 contributes to the dysfunction of vascular endothelial cells by disturbing the activity of endothelial nitric oxide synthase (eNOS) in sepsis[29]. Furthermore, ARG1 is a marker of the M2 phenotype of macrophages[30]. Cyclin-dependent kinase inhibitor 1C (CDKN1C) is a G1/S phase inhibitor that plays vital roles in limiting cell proliferation[31]. SEC63 is a component of the active posttranslational Sec translocon and participates in the translocation of precursor proteins[32]. However, the role of SEC63 and CDKN1C in sepsis is still unclear and warrants further experimental verification.

Finally, we identified and validated TAL as a candidate drug for sepsis patients by cMap database and in vivo experiments. TAL is a tumor necrosis factor-α (TNF-α) antagonist that exerts potent anti-inflammatory and immunomodulatory effects[33,34]. TAL administration efficiently prevents the progression to sepsis after *Escherichia coli* exposure[35] and considerably prolongs survival in multidrug-resistant *Pseudomonas aeruginosa, Klebsiella pneumoniae B5055*, and LPS-induced sepsis mouse models[36–38]. In the present study, we demonstrated the anti-senescence effect of TAL in mice model of sepsis for the first time. However, the mechanism remains unknown.

Inevitably, the present study has some limitations. First, it was a retrospective study based on public databases. Second, although a total of 2050 sepsis patients and 173 healthy controls were included in the present study, only 479 sepsis patients from the GSE65682 cohort provided prognosis information with survival time. Finally, the prognostic and diagnostic models for sepsis patients need further clinical trials for verification. And further experiments are needed to explore the molecular mechanisms underlying the anti-senescence role of TAL.

In summary, the current study constructed a novel sepsis classification based on the aging-related signature and established prognostic and diagnostic models for sepsis patients. By classifying sepsis into High- and Low-aging groups, this study provided new insights into the heterogeneity of sepsis and shed new light on delivering precision medicine for sepsis patients. TAL is a potential candidate drug for sepsis patients by attenuating LPS induced cellular senescence.

Methods

Data acquisition and data processing

Five gene expression datasets (GSE65682, GSE26440, GSE26378, GSE185263, and GSE95233) and their corresponding clinical data were obtained from the Gene Expression Omnibus (GEO) database (https://www.ncbi.nlm.nih.gov/gds/)[39]. The gene expression dataset and corresponding clinical data of E-MTAB-4421, E-MTAB-5273, and E-MTAB-5274 were obtained from the EMBL-European Bioinformatics Institute (EMBL-EBI) database (https://www.ebi.ac.uk/biostudies/arrayexpress)[40].

A total of 2050 sepsis patients and 173 healthy controls were included in the present study. The GSE65682 cohort comprised 760 sepsis patients and 42 healthy controls. The GSE26440 cohort comprised 98 sepsis patients and 32 healthy controls. The GSE26378 cohort comprised 82 sepsis patients and 21 healthy controls. The GSE65682 cohort comprised 348 sepsis patients and 44 healthy controls. The GSE95233 cohort comprised 102 sepsis patients and 22 healthy controls. The E-MTAB-5273 cohort comprised 277 sepsis patients and 10 healthy controls. The E-MTAB-5274 and E-MTAB-4421 cohorts only comprised 108 and 270 sepsis patients, respectively, which were utilized to validation the prognostic value of the and GOBP_AGING score and prognostic model, respectively. Since both GSE26440 and GSE26378 were derived from Wong et al.[41,42] based on the GPL570 platform, a metadata cohort named GSE26440-26378 was created by merging the two microarray datasets, and batch effects were removed using the combat function in the SVA R package[43].

Additionally, single-cell RNA-sequencing (scRNA-seq) data on human peripheral blood mononuclear cell (PBMC) samples from 2 healthy controls and 5 sepsis patients at 0 h postdiagnosis were retrieved from GSE167363. Detailed information on the cohorts included in the present study is shown in Supplementary table 1.

Gene set variation analysis

Gene set variation analysis (GSVA) is a method that estimates the variation in pathway activity over a sample population in an unsupervised manner[44]. The GSVA package was used to estimate GSVA scores for each gene set based on the reference gene sets from c5.go.bp.v2023.1.Hs.symbols.gmt consisting of 7751 biological process gene sets, c2.cp.v2023.1.Hs.symbols.gmt consisting of 50 hallmark gene sets, and c2.cp.v2023.1.Hs.symbols.gmt consisting of 3090 canonical pathway gene sets that were obtained from the MsigDB database (http://www.gsea-msigdb.org/gsea/msigdb/index.jsp). Then, we used the "limma"[45] and "ComplexHeatmap"[46] packages to display distinct pathways between normal and sepsis patients or among different sepsis subgroups.

Single-cell RNA-seq analysis

We utilized the Seurat R package and applied standard downstream processing for scRNA-seq data as previously described[47]. Briefly, data normalization was first conducted using the LogNormalize method. Then, the "FindVariableFeatures" (selection.method = "vst", nfeatures = 3000) and "FindIntegrationAnchors" functions were used to select features and anchors for downstream integration. After integration, cells with ≥ 500 genes or with a mitochondrial gene ratio ≤ 5% were regarded as high-quality cells for further analysis. After data integration and scaling, the "RunPCA" and "FindClusters" functions were utilized for principal component analysis (PCA) and clustering. The "RunUMAP" function was then used for dimensionality reduction with a resolution of 0.5 to calculate the top 30 dimensions. Subsequently, the "FindAllMarkers" function was used to identify marker genes for each cluster (adjusted $P < 0.05$). Afterward, the annotation of cell type was conducted using ToppGeneSuit (https://toppgene.cchmc.org/), CellMarker (http://xteam.xbio.top/CellMarker/), and PanglaoDB (https://panglaodb.se/search.html) databases.

Molecular characteristics of sepsis subclasses

The differentially expressed genes (DEGs) between the two subgroups were identified using the "limma" package in R with cutoff criteria of an adjusted P value < 0.05. Functional enrichment analysis of cluster-specific DEGs was conducted using the Metascape database (https://Metascape.org/). $P < 0.05$ was considered statistically significant. GSVA was then employed to estimate the score of the 50 hallmark gene sets. After that, we used the "ComplexHeatmap" R package to display distinct pathways between the High- and Low-aging groups.

Moreover, nearest template prediction (NTP) analysis[48] was used to predict the correlation between previously published sepsis endotypes and our classification.

Estimation of immune cell infiltration and immune function

To further explore the difference in immune cell infiltration between the two groups, single-sample GSEA (ssGSEA) was used to estimate immune infiltration based on 184 immune cell and immune function signatures collected by Wang et al.[49] by computing an enrichment score representing the degree of immune infiltration within a single sample.

Establishment of prognostic and diagnostic models

To establish the prognostic model, the aging-related prognostic DEGs for sepsis patients were first identified. The DEGs of sepsis patients compared to healthy controls from GSE68652, GSE185263, GSE95233, and GSE26440-26378 were first intersected to obtain the common DEGs (sepsis/normal). Then, the prognostic genes of sepsis were identified by univariate Cox regression[50]. Finally, the aging-related prognostic DEGs for sepsis patients were identified by inserting common DEGs, prognostic genes, and members of the GOBP_AGING gene set.

Afterward, since only the GSE68652 cohort had detailed survival information among the included cohorts in the present study, the tenfold LASSO cross-validation Cox regression analysis[13] was applied to selected key aging-related prognostic DEGs. LASSO is a regression method for multiple parameters[13]. In tenfold cross-validation, the samples are divided into 10 subsets (folds); each time, nine subsets are used to train the model, and then the remaining subset is used for validation. After the screening of key genes, we constructed a prognostic model using the ratio of up-regulated genes to down-regulated genes. The predictive ability of the model for the cohort was evaluated using the Kaplan–Meier log-rank test[50] and time-dependent receiver operating characteristic (ROC) curve analysis[51].

Identifying candidate drugs for sepsis patients based on aging-related DEGs

To identify candidate drugs for k sepsis patients based on aging-related DEGs, the aging-related DEGs were first identified by inserting common DEGs and members of the GOBP_AGING gene set. Then, the up- and down-regulated sepsis-DEGs were submitted into the cMap (Connectivity map) (https://clue.io/). cMap is a database of small-molecule drugs, gene expression profiles, and diseases that is based on the differential gene expression of human cells treated with well-defined compounds. All compounds are assigned a connectivity score (ranging from −100 to 100) based on the similarity of the gene expression changes they induce when compared to the given gene set. The positive connectivity score illustrates that the drug is capable of inducing similar gene expression changes to those in the uploaded set, while negative scores indicate opposing patterns. Therefore, the most negatively correlated launched compounds were screened for sepsis patients.

Reagents

Thalidomide (TAL) was purchased from MedChemExpress CO., Ltd (Shanghai, China), Lipopolysaccharide was purchased from Beyotime (Shanghai, China). IL-1β and TNF-α ELISA Kits were purchased from Bioawamp (Wuhan, China). Antibodies against GAPDH, and β-Galactosidase were purchased from Proteintech (Illinois, USA); and antibodies against p16 and p21 were purchased from Abcam (Cambridge, UK).

Ethics statement

All animal experimental procedures were performed in accordance with the ARRIVE guidelines (https://arriveguidelines.org) and American Veterinary Medical Association (AVMA) Guidelines for the Euthanasia of Animals (2020). Moreover, all animal experimental procedures were approved by the Animal Ethical Committee of Tongji Medical College, Huazhong University of Science and Technology ([2024] IACUC Number: 3991).

Experimental animals

C57BL/6 mice (6–8 weeks old) were purchased from Beijing Huafukang Bioscience Co. Inc. (Beijing, China) and housed in the Animal Care Facility of Tongji Medical College at 25 °C, 45–75% relative humidity, and in 12/12 h

dark/light conditions. After a 1-week adaptive phase, all mice were randomly divided into two groups: NC group (negative control), LPS group (10 mg/kg i.p.), TAL group (50 mg/kg i.p. 1 h before LPS injection). 24 h after LPS injection, mice were euthanized by cervical dislocation for the collection of the blood and livers.

Hematoxylin and eosin (HE) and immunohistochemistry (IHC)

Formalin-fixed lung and kidney specimens were embedded in paraffin blocks and cut into 5 μm sections. The sections were then stained with hematoxylin and eosin for histology.

The damage assessment was carried out by two researchers who did not know the experimental design. The histological assessment of lung damage was based on a lung injury scoring system[52]. The histological assessment of kidney damage included the loss of the tubule brush border, tubular casts, tubular necrosis, tubular hemorrhage, and inflammatory infiltration. The scoring principle was as follows: 0, no damage; 1, ≤ 10% damage; 2, 11–25% damage; 3, 26–45% damage; 4, 46–75% damage, and 5, ≥ 76% damage[53].

For IHC, the sections were deparaffinized and rehydrated with ethanol and xylene and then heated to 95 °C for 20 min in 10 mM citrate buffer, pH 6.0. After a blocking step with PBS containing 10% goat serum for 1 h at room temperature, the sections were incubated with a primary antibody 1:200 p16 (Proteintech, 10883-1-AP), and p21 (Proteintech, 10355-1-AP) overnight at 4 °C. Subsequently, the sections were incubated with biotinylated goat anti-rabbit IgG. After incubation with secondary antibodies, the sections were mounted and evaluated with an Olympus microscope. For the quantitative expression of p16 and p21, the density of the immunoreactive proteins was analyzed by ImageJ software.

Enzyme-linked immunosorbent assay (ELISA)

The protein levels of serum IL-1β and TNF-α were tested by using mouse IL-1β (Bioswamp, MU30369) and TNF-α (Bioswamp, MU30030) ELISA kits according to the manufacturer's instructions as previously described[54].

Serum creatinine (SCr) and BUN test

The serum Creatinine (SCr) and BUN were tested by using creatinine and urea assay kits (Nanjing Jiancheng, C011-2-1 and C013-2-1) according to the manufacturer's instructions.

Western blot analysis

Kidney proteins were extracted using cold RIPA buffer containing PMSF. Total proteins were loaded onto SDS-PAGE gels, separated by electrophoresis, and transferred onto PVDF membranes. After a blocking step in Tris-buffered saline plus Tween 20 (TBS-T) solution containing 5% nonfat milk for 1 h, the membranes were incubated with KIM-1 (Proteintech, 30948-1-AP) or NGAL (Proteintech, 26991-1-AP) antibodies overnight at 4 °C. After three washes with TBST, the membranes were incubated at 37 °C with HRP-linked secondary antibody for 1 h. Enhanced chemiluminescent substrate was used to visualize the immune bands.

Statistical analysis

All computational and statistical analyses were performed using R programming (https://www.r-project.org/) and SPSS 22.0 (IBM Corp., ArmRonk, NY, USA). The histogram, Q–Q plot, Kolmogorov–Smirnov test, and Shapiro-Wilks's test were employed to test the normality of data[55]. To compare two or three groups with normally distributed variables, unpaired Student's t test and one-way ANOVA were utilized, respectively[56]. Kruskal–Wallis test was employed to compare three groups with nonnormal distribution parameters[57]. The chi-square test was used to analyze contingency table variables[58]. Survival analysis was performed using Kaplan–Meier methods with the log-rank test[50]. A two-tailed P value < 0.05 was considered statistically significant.

Data availability

The datasets analyzed during the current study are available in the Gene Expression Omnibus (GEO) database (https://www.ncbi.nlm.nih.gov/gds/) and EMBL-European Bioinformatics Institute (EMBL-EBI) database (https://www.ebi.ac.uk/biostudies/arrayexpress). The datasets used and/or analyzed during the current study are available from the corresponding author on reasonable request.

Received: 22 September 2024; Accepted: 11 December 2024
Published online: 28 December 2024

References

1. Komorowski, M., Green, A., Tatham, K. C., Seymour, C. & Antcliffe, D. Sepsis biomarkers and diagnostic tools with a focus on machine learning. *EBioMedicine* **86**, 104394 (2022).
2. Baghela, A. et al. Predicting sepsis severity at first clinical presentation: The role of endotypes and mechanistic signatures. *EBioMedicine* **75**, 103776 (2022).
3. Scicluna, B. P. et al. Classification of patients with sepsis according to blood genomic endotype: a prospective cohort study. *Lancet Respir. Med.* **5**, 816–826 (2017).
4. Davenport, E. E. et al. Genomic landscape of the individual host response and outcomes in sepsis: a prospective cohort study. *Lancet Respir. Med.* **4**, 259–271 (2016).
5. Merdji, H., Schini-Kerth, V., Meziani, F. & Toti, F. Long-term cardiovascular complications following sepsis: is senescence the missing link?. *Ann. Intensive Care* **11**, 166 (2021).
6. Kim, C. O., Huh, A. J., Han, S. H. & Kim, J. M. Analysis of cellular senescence induced by lipopolysaccharide in pulmonary alveolar epithelial cells. *Arch. Gerontol. Geriatr.* **54**, e35-41 (2012).
7. Yu, H. M. et al. Repeated lipopolysaccharide stimulation induces cellular senescence in BV2 cells. *Neuroimmunomodulation* **19**, 131–136 (2012).
8. Zhao, M. & Chen, X. Effect of lipopolysaccharides on adipogenic potential and premature senescence of adipocyte progenitors. *Am. J. Physiol. Endocrinol. Metab.* **309**, E334–E344 (2015).

9. Feng, X. et al. Repeated lipopolysaccharide stimulation promotes cellular senescence in human dental pulp stem cells (DPSCs). *Cell Tissue Res.* **356**, 369–380 (2014).
10. Li, H. et al. Pseudomonas aeruginosa induces cellular senescence in lung tissue at the early stage of two-hit septic mice. *Pathog. Dis.* **76**, ftz001 (2018).
11. Oliveira, N. M. et al. Sepsis induces telomere shortening: a potential mechanism responsible for delayed pathophysiological events in sepsis survivors?. *Mol. Med.* **22**, 886–891 (2017).
12. Merdji, H. et al. Septic shock as a trigger of arterial stress-induced premature senescence: A new pathway involved in the post sepsis long-term cardiovascular complications. *Vascul. Pharmacol.* **141**, 106922 (2021).
13. Tibshirani, R. Regression shrinkage and selection via the lasso. *J. R. Stat. Soc. Ser. B Stat. Methodol.* **58**, 267–288 (1996).
14. Liberzon, A. et al. The molecular signatures database (MSigDB) hallmark gene set collection. *Cell Syst.* **1**, 417–425 (2015).
15. Hughes, G. Youden's index and the weight of evidence. *Methods Inf. Med.* **54**, 198–199 (2015).
16. Stanski, N. L. & Wong, H. R. Prognostic and predictive enrichment in sepsis. *Nat. Rev. Nephrol.* **16**, 20–31 (2020).
17. Hartman, C. L. & Ford, D. A. MPO (*Myeloperoxidase*) caused endothelial dysfunction. *Arterioscler. Thromb. Vasc. Biol.* **38**, 1676–1677 (2018).
18. Liu, W. Q. et al. Myeloperoxidase-derived hypochlorous acid promotes ox-LDL-induced senescence of endothelial cells through a mechanism involving β-catenin signaling in hyperlipidemia. *Biochem. Biophys. Res. Commun.* **467**, 859–865 (2015).
19. Kothari, N. et al. Increased myeloperoxidase enzyme activity in plasma is an indicator of inflammation and onset of sepsis. *J. Crit. Care* **26** (435), e1–7 (2011).
20. Meyer, N. J. et al. Myeloperoxidase-derived 2-chlorofatty acids contribute to human sepsis mortality via acute respiratory distress syndrome. *JCI Insight* https://doi.org/10.1172/jci.insight.96432 (2017).
21. Nalivaeva, N. N., Zhuravin, I. A. & Turner, A. J. Neprilysin expression and functions in development, ageing and disease. *Mech. Ageing Dev.* **192**, 111363 (2020).
22. Lu, B. et al. Neutral endopeptidase modulation of septic shock. *J. Exp. Med.* **181**, 2271–2275 (1995).
23. Martens, A., Eppink, G. J., Woittiez, A. J., Eidhof, H. & de Leij, L. F. Neutrophil function capacity to express CD10 is decreased in patients with septic shock. *Crit. Care Med.* **27**, 549–553 (1999).
24. Guérin, E. et al. Circulating immature granulocytes with T-cell killing functions predict sepsis deterioration*. *Crit. Care Med.* **42**, 2007–2018 (2014).
25. Drifte, G., Dunn-Siegrist, I., Tissières, P. & Pugin, J. Innate immune functions of immature neutrophils in patients with sepsis and severe systemic inflammatory response syndrome. *Crit. Care Med.* **41**, 820–832 (2013).
26. Munder, M. et al. Suppression of T-cell functions by human granulocyte arginase. *Blood* **108**, 1627–1634 (2006).
27. Zhang, J. X. et al. ARG1 as a promising biomarker for sepsis diagnosis and prognosis: evidence from WGCNA and PPI network. *Hereditas* **159**, 27 (2022).
28. Ahmad, S. et al. Transcriptome meta-analysis deciphers a dysregulation in immune response-associated gene signatures during sepsis. *Genes (Basel)* **10**, 1005 (2019).
29. Hu, S. et al. Disrupted eNOS activity and expression account for vasodilator dysfunction in different stage of sepsis. *Life Sci.* **264**, 118606 (2021).
30. Orecchioni, M., Ghosheh, Y., Pramod, A. B. & Ley, K. Macrophage polarization: Different gene signatures in M1(LPS+) vs. classically and M2(LPS-) vs. alternatively activated macrophages. *Front. Immunol.* **10**, 1084 (2019).
31. Matsuoka, S. et al. p57KIP2, a structurally distinct member of the p21CIP1 Cdk inhibitor family, is a candidate tumor suppressor gene. *Genes Dev.* **9**, 650–662 (1995).
32. Itskanov, S., Kuo, K. M., Gumbart, J. C. & Park, E. Stepwise gating of the Sec61 protein-conducting channel by Sec63 and Sec62. *Nat. Struct. Mol. Biol.* **28**, 162–172 (2021).
33. Majumder, S., Sreedhara, S. R., Banerjee, S. & Chatterjee, S. TNF α signaling beholds thalidomide saga: a review of mechanistic role of TNF-α signaling under thalidomide. *Curr. Top. Med. Chem.* **12**, 1456–1467 (2012).
34. Zhu, Y. X., Kortuem, K. M. & Stewart, A. K. Molecular mechanism of action of immune-modulatory drugs thalidomide, lenalidomide and pomalidomide in multiple myeloma. *Leuk. Lymphoma* **54**, 683–687 (2013).
35. Giamarellos-Bourboulis, E. J. et al. Effective immunomodulatory treatment of *Escherichia coli* experimental sepsis with thalidomide. *Antimicrob. Agents Chemother.* **47**, 2445–2449 (2003).
36. Giamarellos-Bourboulis, E. J. et al. Immunomodulatory intervention in sepsis by multidrug-resistant Pseudomonas aeruginosa with thalidomide: an experimental study. *BMC Infect. Dis.* **5**, 51 (2005).
37. Kumar, V., Harjai, K. & Chhibber, S. A combination of thalidomide and augmentin protects BALB/c mice suffering from Klebsiella pneumoniae B5055-induced sepsis. *J. Chemother.* **21**, 159–164 (2009).
38. İlhan, N., Susam, S., Gül, H. F. & İlhan, N. The therapeutic effects of thalidomide and etanercept on septic rats exposed to lipopolysaccharide. *Ulus. Travma Acil Cerrahi Derg.* **25**, 99–104 (2019).
39. Clough, E. & Barrett, T. The gene expression omnibus database. *Methods Mol. Biol.* **1418**, 93–110 (2016).
40. Thakur, M. et al. EMBL's European bioinformatics institute (EMBL-EBI) in 2023. *Nucleic Acids Res.* **52**, D10–d17 (2024).
41. Wong, H. R. et al. Corticosteroids are associated with repression of adaptive immunity gene programs in pediatric septic shock. *Am. J. Respir. Crit. Care Med.* **189**, 940–946 (2014).
42. Wong, H. R. et al. Identification of pediatric septic shock subclasses based on genome-wide expression profiling. *BMC Med.* **7**, 34 (2009).
43. Leek, J. T., Johnson, W. E., Parker, H. S., Jaffe, A. E. & Storey, J. D. The sva package for removing batch effects and other unwanted variation in high-throughput experiments. *Bioinformatics* **28**, 882–883 (2012).
44. Hänzelmann, S., Castelo, R. & Guinney, J. GSVA: gene set variation analysis for microarray and RNA-seq data. *BMC Bioinform.* **14**, 7 (2013).
45. Ritchie, M. E. et al. limma powers differential expression analyses for RNA-sequencing and microarray studies. *Nucleic Acids Res.* **43**, e47 (2015).
46. Gu, Z. & Hübschmann, D. Make interactive complex heatmaps in R. *Bioinformatics* **38**, 1460–1462 (2022).
47. Zhang, T. et al. A novel liver zonation phenotype-associated molecular classification of hepatocellular carcinoma. *Front. Immunol.* **14**, 1140201 (2023).
48. Hoshida, Y. Nearest template prediction: a single-sample-based flexible class prediction with confidence assessment. *PLoS One* **5**, e15543 (2010).
49. Wang, S. et al. Clinical significance and immunogenomic landscape analyses of the immune cell signature based prognostic model for patients with breast cancer. *Br. Bioinform.* https://doi.org/10.1093/bib/bbaa311 (2021).
50. Abd ElHafeez, S. et al. An overview on standard statistical methods for assessing exposure-outcome link in survival analysis (Part II): the Kaplan-Meier analysis and the Cox regression method. *Aging Clin. Exp. Res.* **24**, 203–206 (2012).
51. Cao, R. & López-de-Ullibarri, I. ROC curves for the statistical analysis of microarray data. *Methods Mol. Biol.* **1986**, 245–253 (2019).
52. Matute-Bello, G. et al. An official American thoracic society workshop report: features and measurements of experimental acute lung injury in animals. *Am. J. Respir. Cell Mol. Biol.* **44**, 725–738 (2011).
53. Zhao, X. et al. Three-dimensional aggregates enhance the therapeutic effects of adipose mesenchymal stem cells for ischemia-reperfusion induced kidney injury in rats. *Stem Cells Int.* **2016**, 9062638 (2016).

54. Zhang, T. & Gu, J. Renalase attenuates mouse fatty liver ischemia/reperfusion injury through mitigating oxidative stress and mitochondrial damage via activating SIRT1. *Oxid. Med. Cell. Longev.* **2019**, 7534285 (2019).
55. Vetter, T. R. Fundamentals of research data and variables: The devil is in the details. *Anesth. Analg.* **125**, 1375–1380 (2017).
56. Hazra, A. & Gogtay, N. Biostatistics series module 3: Comparing groups: Numerical variables. *Indian J. Dermatol.* **61**, 251–260 (2016).
57. Kruskal, W. H. & Wallis, W. A. Use of ranks in one-criterion variance analysis. *J. Am. Stat. Assoc.* **47**, 583–621 (1952).
58. Pandis, N. The chi-square test. *Am. J. Orthod. Dentofac. Orthop.* **150**, 898–899 (2016).

Author contributions

Tao Zhang and Yingli Nie designed this work. Kai Yang and Yaoyao Lu integrated and analyzed the data. Yaoyao Lu and Jian Gu performed animal experiments. Kai Yang and Yingli Nie wrote this manuscript. Tao Zhang critically revised the manuscript for important intellectual content, obtained funding, and provided supervision. All authors contributed to the article and approved the submitted version.

Funding

This work was supported by the National Natural Science Foundation of China (Grant No. 82200972).

Declarations

Competing interests

The authors declare no competing interests.

Additional information

Supplementary Information The online version contains supplementary material available at https://doi.org/10.1038/s41598-024-83111-1.

Correspondence and requests for materials should be addressed to Y.N. or T.Z.

Reprints and permissions information is available at www.nature.com/reprints.

Publisher's note Springer Nature remains neutral with regard to jurisdictional claims in published maps and institutional affiliations.